Lumped Compensation of Nonlinearities based on Optical Phase Conjugation

Kaminski, Pawel Marcin; Daros, Francesco; Yankov, Metodi Plamenov; Hansen, Henrik Enggaard; Ulvenberg, Johan Bertram Thjalfe; Schou, Christian Koefoed; Porto da Silva, Edson; Sutili, Tiago; Junior, Jose Helio; Simoes, Glauco C.C.P.

Total number of authors:
15

Published in:
Journal of Lightwave Technology

Link to article, DOI:
10.1109/JLT.2021.3121435

Publication date:
2022

Document Version
Peer reviewed version

This article has been accepted for publication in a future issue of this journal, but has not been fully edited. Content may change prior to final publication. Citation information: DOI 10.1109/JLT.2021.3121435, Journal of Lightwave Technology

Lumped Compensation of Nonlinearities based on Optical Phase Conjugation

P.M. Kaminski, F. Da Ros, M.P. Yankov, H.E. Hansen, J.B.T. Ulvenberg, C.K. Schou, E.P. da Silva, T. Sutili, J.H. da Cruz Júnior, G.C.C.P. Simões, A.T. Clausen, S. Forchhammer, R.C. Figueiredo, L.K. Oxenløwe, and M. Galili

Abstract—Compensation of Kerr nonlinearity-induced distortions has been shown to allow for increasing transmission rate and reach, with optical compensation techniques particularly attractive for broadband wavelength-division multiplexed (WDM) scenarios. However, they normally require additional devices within the link, which is particularly challenging for already deployed systems, and even more so for unrepeatered transmission. In this work, we focus on providing lumped optical nonlinearity suppression, either at the transmitter or at the receiver side, based on optical phase conjugation (OPC). The theory to design scaled-down OPC compensation modules is derived, and it allows to move beyond the standard mid-link OPC approach and to explore compensation modules with fibers types not directly linked to the dispersion properties of the transmission link. This design method is then validated both through numerical investigations and experimental demonstrations for a number of systems with a varying degree of complexity. Ultimately, significant performance improvement is shown by employing short OPC-based compensation structures which are carefully designed to match much longer transmission links.

Index Terms—four-wave mixing, optical-phase-conjugation, quadrature-amplitude-modulation, coherent communications.

I. Introduction

OPTICAL communication systems are the backbone of our entire communication infrastructure, and they need to keep evolving to follow the steadily increasing demand for connectivity. Whereas radical paradigm shifts such as multi-band transmission and space-division multiplexing (SDM) [1] are being researched upon and show significant promise in providing multiplicative factors to the achievable throughput, these approaches will require time for developing new hardware and network control techniques. It is therefore crucial to still focus on maximizing the throughput of existing systems [2], as the developed solution will not only help on the short term, but may also be portable to future multi-band and SDM systems [3]. One of the key challenges currently limiting the system throughput is the nonlinear distortion introduced by the interplay between the Kerr nonlinearity and the fiber dispersion [2]. Consequently, digital pre- and post-compensation methods have been proposed and are particularly effective to compensate for intra-channel nonlinearity [2], [4], whereas compensation directly in the optical domain also enables addressing inter-channel nonlinearity as in [2], [4], [5]. Among the optical techniques, optical phase conjugation (OPC) has shown a particular promise, though it relies on a certain degree of propagation symmetry within the transmission link. Still, several works in the literature have previously shown its significant benefits for optical systems [2], [5]–[14], even within a network scenario with randomly placed OPC operations [17]. The results required the ability to insert an OPC module within the transmission link and, to some degree, the manipulation of the existing links. Both of these requirements are challenging to satisfy for deployed systems, especially in unrepeatered transmission, where the link can only be accessed at its end-points and no additional active elements can be added in the middle.

In order to address links where mid-link access is challenging, it would be beneficial to provide nonlinearity compensation in the optical domain through pre- or post-compensation, similarly to digital approaches. Preliminary works in this direction have been reported in [18]–[20] where the numerical analysis relied on specifically designed fibers, either dispersion-decreasing [18] or dispersion-varying [19], neither of which is currently commercially available. The use of dispersion-compensating fiber (DCF) in conjunction with optimized Raman amplification has also been numerically proposed in [21], but it was only shown suitable for non-standard links based on transmission fibers with a negative dispersion sign, i.e. negative dispersion for both compensator and transmission link. This choice substantially limits the applicability of this approach. Alternatively, experimental demonstrations of pre-compensation have been reported in [22], [23], though they were focused on multi-span systems, and could only achieve limited propagation symmetry.

In this paper, we extend our previous work in [24]–[26] to provide an overview of OPC-based pre- or post-compensation of Kerr-induced signal distortions in unre-

P.M. Kaminski was with the Department of Photonics Engineering, Technical University of Denmark, Kongens Lyngby, 2800 Denmark. He is now with the VPI Photonics, Berlin, 10587 Germany.

F. Da Ros, M.P. Yankov, H.E. Hansen, J.B.T. Ulvenberg, C.K. Schou, A.T. Clausen, S. Forchhammer, L.K. Oxenløwe and M. Galili are with the Department of Photonics Engineering, Technical University of Denmark, Kongens Lyngby, 2800 Denmark, e-mail: fdro@fotonik.dtu.dk.

E.P. da Silva was with the Department of Photonics Engineering, Technical University of Denmark, Kongens Lyngby, 2800 Denmark. He is now with the Department of Electrical Engineering, Federal University of Campina Grande (UFCG), Campina Grande, 58429-900 Brazil.

T. Sutili, J.H. da Cruz Júnior, G.C.C.P. Simões and R.C. Figueiredo are with Optical Communication Solutions, CPQD, Campinas/SP, 13086-902 Brazil.

This article has been accepted for publication in a future issue of this journal, but has not been fully edited. Content may change prior to final publication. Citation information: DOI 10.1109/JLT.2021.3121435, Journal of Lightwave Technology

Fig. 1. Schematics of a simple two-span transmission system including OPC: signal (left, L_1), and conjugate (righ, L_2).

peatered systems. The separate results of [24]–[26] are put into perspective through a complete theoretical discussion and additional numerical investigations. The remainder of this paper is organized as follows. Section II presents a novel approach to the OPC compensation requirements by relaxing the need for compensation to occur in the opposite order as the original nonlinear distortion. It also compares the proposed approach with the standard method commonly used and discusses general guidelines on how to construct a lumped compensation module to satisfy them. The theoretical analysis is confirmed by idealized numerical investigations, i.e. neglecting practical limitations, that would hinder the compensation, to focus only on the link designed following the proposed method, as well as experimental validations where practical limitations are considered to confirm that significant gains are still achievable. Section III contains both numerical and experimental validations of OPC-based post-compensation where the proposed method is applied to systems with different dispersion profiles. Additionally, Section III also contains a numerical validation of the post compensation scheme applied to a state-of-the-art unrepeatered link. Finally, the conclusions are drawn in Section IV.

II. OPC compensation requirements

The general idea behind OPC-based compensation is illustrated in Fig. 1, where the link consists of two fiber spans with an OPC device in the middle. For such a system, the compensation technique can be summarized in three steps:

1) accumulation of nonlinearities in the first span;
2) reversing the sign of the accumulated nonlinearities by OPC;
3) applying additional nonlinearities in the second span.

The compensation is successful if the nonlinearities in both spans are identical, and if they are indeed reversed by OPC. With both conditions satisfied, the degrading impact of the nonlinearity is suppressed, and so the system performance is expected to increase dramatically. This same reasoning can be applied to standard two-span systems with mid-link OPC, but also to unrepeatered links where one side of the OPC is lumped and located at the transmitter or the receiver.

To derive the compensation criteria, we refer to the nonlinear Schröedinger equation (NLSE), which incorporates the key propagation characteristics, i.e. the fiber loss, the group velocity dispersion and the Kerr nonlinearity [27], [28]:

$$\frac{d}{dz}A(z,t) = \left(-i\frac{1}{2}\beta_2\frac{d^2}{dt^2} + i\gamma|A(z,t)|^2 - \frac{\alpha}{2}\right)A(z,t). \quad (1)$$

The NLSE can then be reformulated to a more convenient form using a set of operators:

$$\frac{d}{dz}A(z,t) = \left(i\hat{D} + i\hat{N} + \hat{L}\right)A(z,t), \quad (2)$$

where:

$$\hat{D} = -\frac{1}{2}\beta_2\frac{d^2}{dt^2}, \quad (3)$$

$$\hat{N} = +\gamma|A(z,t)|^2, \quad (4)$$

$$\hat{L} = -\frac{\alpha}{2}. \quad (5)$$

Using Eq. (2), the complex field amplitude A has the following form after transmission in the first span (left of OPC):

$$A(L_1,t) = \exp\left[\int_0^{L_1}\left(iD_1 + i\hat{N}_1 + \hat{L}_1\right)dz\right]A(0,t), \quad (6)$$

where the subscripts on the operators indicate in which part of the link (span 1 or span 2) the effects have been experienced. After propagation in the first span, the field is conjugated using OPC and the phase distortions are reversed, resulting in:

$$A^*(L_1,t) = \exp\left[\int_0^{L_1}\left(-i\hat{D}_1 - i\hat{N}_1 + \hat{L}_1\right)dz\right]A^*(0,t). \quad (7)$$

Finally, the signal is transmitted through the second span (right side of the OPC, in Fig. 1), and it accumulates additional impairments as a consequence of propagation:

$$A(L_1+L_2,t) = \\ = \exp\left[\int_{L_1}^{L_1+L_2}\left(i\hat{D}_2 + i\hat{N}_2 + \hat{L}_2\right)dz\right]A^*(L_1,t). \quad (8)$$

For this simple system, the output and input fields are therefore related as:

$$A(L_1+L_2,t) = \exp\left[\int_{L_1}^{L_1+L_2}\left(i\hat{D}_2 + i\hat{N}_2 + \hat{L}_2\right)dz\right] \\ \exp\left[\int_0^{L_1}\left(-i\hat{D}_1 - i\hat{N}_1 + \hat{L}_1\right)dz\right]A^*(0,t), \quad (9)$$

The operators D and L act independently, though they are both intrinsically coupled with the operator N. In

This article has been accepted for publication in a future issue of this journal, but has not been fully edited. Content may change prior to final publication. Citation information: DOI 10.1109/JLT.2021.3121435, Journal of Lightwave Technology

order to separate the transmission integrals, we have to neglect this coupling, and thus we make the following assumption:

$$\int^{L} \left(i\hat{D} + i\hat{N} + \hat{L}\right) dz \approx \approx \int^{L} i\hat{D}\, dz + \int^{L} i\hat{N}\, dz + \int^{L} \hat{L}\, dz. \quad (10)$$

This is a typical assumption for solving the NLSE with the Split-Step Fourier Method (SSFM) [28], [29], and it corresponds to grouping the $\hat{D}$ and $\hat{L}$, operators and ignoring the commutators between them and the $\hat{N}$ operator in the Baker-Hausdorff expansion [28], [30]. This approximation allows for a simple analytical investigation of the system. In the following, we confirm numerically and experimentally that the error caused by neglecting the commutators does not significantly affect the validity of symmetry investigations using this simplified approach.

Under this condition, the integrals from Eq. (9) can be grouped with respect to the underlying physical effects, which helps illustrate the impact of OPC:

$$A(L_1+L_2,t) \approx \exp\left[\left(\int_0^{L_1} \hat{L}_1\, dz + \int_{L_1}^{L_1+L_2} \hat{L}_2\, dz\right) + i\left(\int_0^{L_1} -\hat{D}_1\, dz + \int_{L_1}^{L_1+L_2} \hat{D}_2\, dz\right) + i\left(\int_0^{L_1} -\hat{N}_1\, dz + \int_{L_1}^{L_1+L_2} \hat{N}_2\, dz\right)\right] A^*(0,t).$$

It follows from the above equation that the complex field amplitude at the end of the system can be an exact replica of the input, except for the conjugation, if the respective transmission impairments between the two spans cancel out. That is:

$$A(L_1+L_2,t) = A^*(L_0,t), \quad (11)$$

if the following conditions are met:

$$\int_0^{L_1} \hat{L}_1\, dz = -\int_{L_1}^{L_1+L_2} \hat{L}_2\, dz, \quad (12)$$

$$\int_0^{L_1} \hat{D}_1\, dz = \int_{L_1}^{L_1+L_2} \hat{D}_2\, dz, \quad (13)$$

$$\int_0^{L_1} \hat{N}_1\, dz = \int_{L_1}^{L_1+L_2} \hat{N}_2\, dz. \quad (14)$$

Finally, these requirements can then be explicitly expressed with regard to the fiber characteristics of each of the two spans, as in:

$$\int_0^{L_1} \alpha_1\, dz = -\int_{L_1}^{L_1+L_2} \alpha_2\, dz, \quad (15)$$

$$\int_0^{L_1} \beta_{2,1}\, dz = \int_{L_1}^{L_1+L_2} \beta_{2,2}\, dz, \quad (16)$$

$$\int_0^{L_1} \gamma_1 |A(z,t)|^2\, dz = \int_{L_1}^{L_1+L_2} \gamma_2 |A(z,t)|^2\, dz. \quad (17)$$

Eqs. (15) to (17) separate the OPC requirements with regard to the different physical effects. In Eq. (15), the fiber loss is not impacted by the conjugation, and thus loss (α) in the first span must be compensated with gain ($-\alpha$) in the second span. However, OPC changes the sign of the phase impairments, and so the group velocity dispersion and the nonlinearity have a potential of being cancelled out completely if they are identical in both spans, as shown in Eq. (16) and (17). This reasoning extends to both inter- and intra-channel nonlinearity, as well as dispersion terms of all even orders, which are manifested as imaginary phase-shift in the NLSE, and thus reverse upon conjugation.

Whereas the derivation just outlined initially follows the approach originally proposed by [31], it deviates from such a standard way of designing the compensation by lifting the requirement for the nonlinearity to be compensated in the opposite order of occurrence after the OPC. This requirement is introduced in Eq. (10) in [31], i.e. requiring that $B(-\zeta) = B(\zeta)$, where ζ is the normalized propagation. By focusing on Eq. 17, instead, the requirement on the order of compensation is relaxed. Whereas this approach may be slightly suboptimal for the cases considered by e.g. [31], as the conditions provided by Eq. (13) in [31] did not require to neglect the commutator between nonlinear and linear operators, Eq. 17 allows additional freedom in designing the system. As shown in [25], [32]–[34] and further discussed in the following sections, fibers with opposite signs of dispersion can be considered for the links before and after the OPC. Such links are not fulfilling the condition provided by Eq. (13) in [31] which requires fibers with the dispersion of the same sign for the compensation to take place, as remarked e.g. in [35]. Nevertheless, as numerically analyzed and experimentally validated in the following, effective nonlinearity compensation can still be achieved. Relaxing the requirement on the fiber dispersion has the key advantage of increasing the degrees of freedom to design the link and compensation, e.g. allowing to consider more available fiber types and thus lead to scaled-down compensation modules as discussed in this work.

Ultimately, to compensate the Kerr nonlinearity we focus solely on Eq. (17), and we aim to satisfy it for a number of systems. This objective is generally challenging as the field amplitude $|A(z,t)|$ evolution over distance depends on both its peak power and its normalized pulse power profile in time (referred to simply as pulse shape in the following). Both quantities vary across the transmission link, e.g. due to fiber loss and fiber dispersion, and have to be appropriately engineered for the equation to hold. Consequently, the general formula for the nonlinear phase-shift:

$$\phi_{NL} = \int_{Link} \gamma |A(z,t)|^2\, dz\,, \quad (18)$$

where γ is considered piece-wise constant depending on the span, will require a certain degree of manipulation and new assumptions. In particular, the goal is to match

This article has been accepted for publication in a future issue of this journal, but has not been fully edited. Content may change prior to final publication. Citation information: DOI 10.1109/JLT.2021.3121435, Journal of Lightwave Technology

the nonlinear phase-shifts on both sides of the OPC, while scaling down the length of one side.

III. Link configurations

For standard dispersive systems, the accumulated dispersion induces pulse shape changes, which in turn affect the generated nonlinearity at each point across the link. The pulse shape variations must be accounted for in the symmetry design, and for such systems we design the compensation modules with the ability to provide pulse shape restoration. In this part, we first discuss the design guidelines and introduce a new general metric for the symmetry evaluation in Section III-A, and then we apply it to a wide range of systems. In Section III-B and Section III-C we provide both numerical analysis under idealized conditions and practical experimental validations. The numerical analysis neglects additional noise sources (e.g. low transceiver noise and no OPC noise) and physical effects (polarization-mode dispersion, PMD, and high-order dispersion) that are well-known to hinder the compensation [36] to focus on the validity of the method proposed in Section II. The experimental demonstration, instead, includes the practical noise sources and effects neglected in the numerical analysis, to prove that compensation can still be achieved in real systems. In Section III-B, we aim to compensate standard unrepeatered links based on nonzero dispersion-shifted fibers (NZDSF) and standard single-mode fibers (SSMF), whereas in Section III-C we design and numerically validate the OPC symmetry for state-of-the-art Raman-amplified systems. For all cases, the proposed lumped compensation modules are shown to achieve a high degree of symmetry, and they substantially improve the performance of the analyzed link configurations.

A. Design principles

As dispersion distorts the pulses, the accumulated nonlinear phase-shift must now account for both power and pulse shape evolution. Eq. (18) can be expressed in the following form:

$$\phi_{NL} = \int_{Link} \gamma |A(z,t)|^2 \, dz = \int_{Link} \gamma P(z,t) \, dz. \qquad (19)$$

The symmetry conditions, as given in Eq. (17), are therefore dependent upon the propagating power as a function of both time and distance:

$$\int_0^{L_1} \gamma_1 P(z,t) \, dz = \int_{L_1}^{L_1+L_2} \gamma_2 P(z,t) \, dz. \qquad (20)$$

As a practical tool to illustrate the symmetry of a given system, the power versus accumulated dispersion diagrams (PADDs), proposed e.g. in [37], [38], are often very useful. Under the assumption that the pulse shape is determined only by the accumulated dispersion, the diagrams can indicate whether the same powers are induced at the corresponding pulse shapes, and thus they help evaluate the OPC symmetry. A perfectly symmetric PADD continuously exhibits the same powers at the opposite values of the accumulated dispersion for the signal and the idler, respectively, which in turn implies nonlinearity matching and a high degree of compensation. However, the PADDs only work when identical fiber types are used on both sides of the OPC, and they do not account for the general case where the fibers may be different and even inhomogeneous. Consequently, the use of PADDs is limited when designing lumped compensation structures with scaled-down lengths. To accommodate the general case of diverse fibre properties, we maintain the approximation that the pulse shape is determined by the accumulated dispersion alone, and we then express the nonlinear phase shift versus chromatic dispersion as a metric for determining propagation symmetry:

$$\int_{Link} \gamma P(z,t) \, dz = \int_{Link} \frac{\gamma P(D_{acc})}{D} \, dD_{acc}, \qquad (21)$$

by substituting:

$$D_{acc} = z \cdot D. \qquad (22)$$

Eq. (21) expresses the accumulation of nonlinearity explicitly as a function of accumulated dispersion. The nonlinear phase shift is proportional to transmitted power P and nonlinear coefficient γ, and it is inversely proportional to dispersion D, as the metric quantifies nonlinear phase shift versus pulse broadening due to dispersion rather than physical fiber length L. Instead of targeting the symmetry using PADD, we define a more general metric called nonlinearity versus accumulated dispersion diagram (NADD) based on Eq. (21), and we use it to optimize the symmetry in OPC systems. A symmetric NADD ensures that the total nonlinearity is matched for the same pulse shapes on both sides of the OPC, under the approximation that the pulse shape is determined by dispersion only, and thus it optimizes the degree of compensation. A comparison between PADD and NADD is illustrated in Fig. 2 for a system, which does achieve strong nonlinearity compensation by OPC, despite a highly asymmetric PADD.

The link in Fig. 2a comprises two fiber spans separated by an OPC. In this scheme, the second span is only half the length of the first span, while the magnitude of its dispersion, loss and launch power are doubled and the sign of dispersion is changed. Equivalent pulse propagation is consequently achieved in both spans, where the nonlinearity and pulse shape evolve twice as fast in the second span when seen over physical fibre length. PADD and NADD for this system are shown in Fig. 2b and Fig. 2c, respectively. The PADD is highly asymmetric as the signal power before and after the OPC (right and left, respectively) are substantially different, and thus the map fails to capture the high degree of symmetry which actually exists in this system. The NADD, on the other hand, includes more propagation parameters, and it reveals the symmetry of nonlinearities irrespective of the different fiber lengths. The absolute value in NADD removes the sign of D, as the magnitude of the nonlinearity (y-axis) only depends on

This article has been accepted for publication in a future issue of this journal, but has not been fully edited. Content may change prior to final publication. Citation information: DOI 10.1109/JLT.2021.3121435, Journal of Lightwave Technology

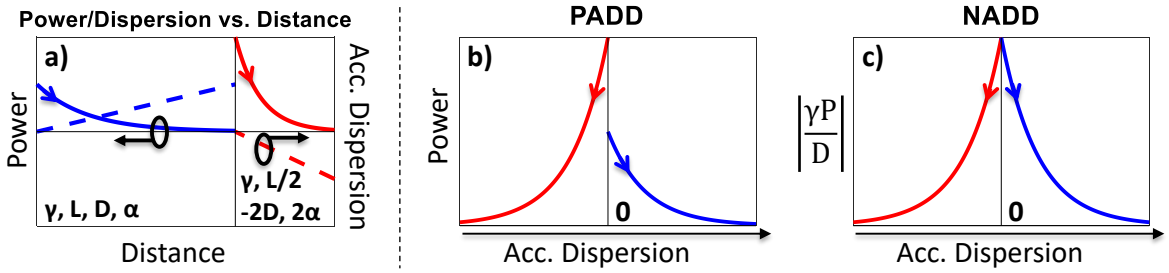

Fig. 2. Two-span symmetric link with unequal launch powers and span lengths (a), with the resulting PADD (b) and NADD (c). Signal and idler are depicted for positive (signal, first part of the link, right-hand side of PADD and NADD) and negative (idler, last part of the link, left-hand side of PADD and NADD) dispersion values, respectively, and the propagation direction is indicated by the arrows. Observe the presence of the dispersion-compensating module (not shown for visual clarity) between the two parts of the links.

the rate of change of accumulated dispersion, though the sign of D is preserved when determining the actual value of accumulated dispersion (x-axis). Moreover, it is noted that the system in Fig. 2 employs fibers with opposite dispersion signs on each side of the OPC, as discussed in [25], [32]–[34]. This allows for the OPC symmetry to be achieved using simple lumped amplification - by e.g. erbium-doped fiber amplifiers (EDFAs), and exponentially decaying power during propagation, as we will show in some of the following demonstrations. In each case, NADDs are used in the analysis of the systems where e.g. scaling, advanced dispersion mapping and fine power profile tuning are simultaneously employed to achieve nonlinear propagation symmetry.

B. Links based on NZDSF and SSMF

In this section, we focus on several types of simple unrepeatered links with exponentially decaying power profiles, and we use NADD to design and optimize lumped optical back-propagation (OBP) modules for receiver-side compensation. For each case, the investigation is conducted using the general setup illustrated in Fig. 3. The transmitter uses C-band laser diodes (LDs) to generate seven wavelength-division multiplexed (WDM) channels on a 25 GHz grid. The channels are modulated with dual-polarization (DP) 16-quadrature-amplitude-modulation (QAM) test data at 16 GBd, combined altogether and amplified. This signal then traverses one of the unrepeatered links, discussed later in more detail, and it is pre-amplified, optically back-propagated, and detected with a coherent receiver. In the end, the signal is processed using a standard digital signal processing (DSP) chain, and its quality is evaluated by means of the received signal to noise ratio (SNR) [39], as given by:

$$< \text{SNR} >= \text{E}_k[|x_k|^2]/\text{E}_k[|y_k - x_k|^2], \qquad (23)$$

where x and y are the transmitted and received symbols, respectively, and k represents a temporal index.

In order to satisfy the OPC symmetry criteria, the compensation module contains three main components:

- dispersion compensating unit for pulse shaping,
- OPC device for reversing the nonlinearity,
- compensation fiber for nonlinearity cancellation.

The dispersion compensating unit is implemented in a completely lumped fashion, whereas the compensation fiber depends on the type of the link. In this section, we analyze three separate link configurations, as follows:

1) NZDSF in the link + SSMF for compensation,
2) NZDSF in the link + DCF for compensation,
3) SSMF in the link + DCF for compensation,

and they are referred to as System1, System2, and System3, respectively. The relevant propagation parameters of each of the employed fiber types are provided in Table I.

TABLE I
Parameters of fibers for dispersive transmission systems at 1550 nm.

Type	α, dB/km	D, ps/nm/km	γ, 1/W/km	L, km
NZDSF	0.2	5.0	1.5	varied
SSMF	0.2	17.0	1.3	varied
DCF	0.5	-100.0	5.4	varied

All three systems are investigated numerically in Section III-B1, and then the approach is verified experimentally for System1 in Section III-B2. In either case, the OBP module is optimized with respect to the OPC symmetry, with the goal of achieving maximum compensation gains.

1) Numerical simulations: First, the three transmission systems are simulated numerically using the setup in Fig. 3, with a few additional assumptions. The lengths of the links are maintained at 200 km in all cases, the OPC is implemented as ideal conjugation of the field, noise figures (NFs) of all EDFAs are set to 5 dB, the transmitter SNR is kept high at 35 dB, and fiber propagation simulation uses SSFM with an adaptive step size [28], [29], while neglecting PMD and higher order dispersion. The optimization of each of the three systems is conducted with respect to the following parameters, all of which determine the degree of symmetry of propagation:

- signal launch power into the link, P_1;
- idler launch power into the compensation fiber, P_2;
- length of the compensation fiber L_2.

These variables are optimized to maximize the received SNR using a standard grid-search method.

This article has been accepted for publication in a future issue of this journal, but has not been fully edited. Content may change prior to final publication. Citation information: DOI 10.1109/JLT.2021.3121435, Journal of Lightwave Technology

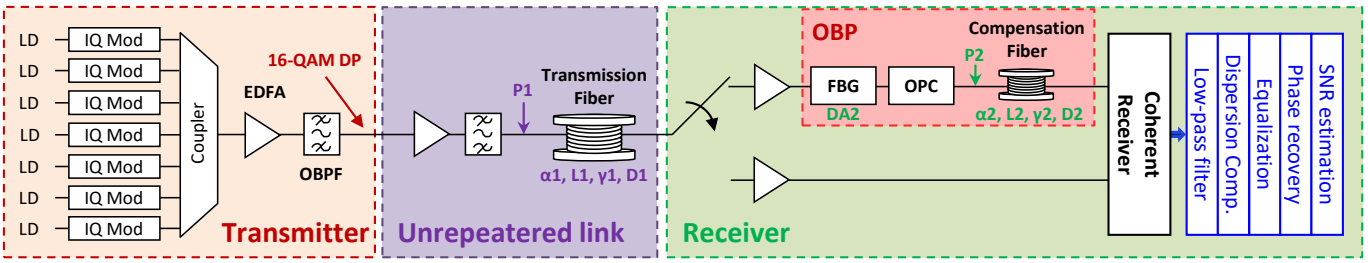

Fig. 3. Configuration of unrepeatered transmission system with and without OBP.

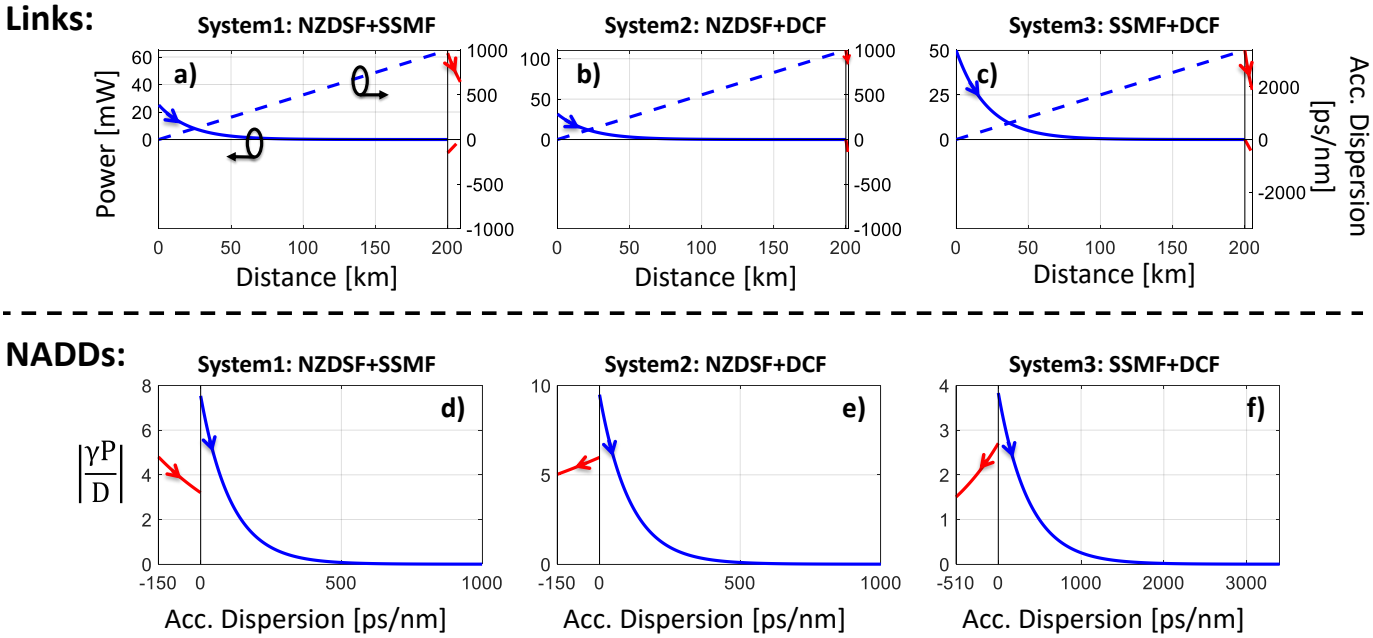

Fig. 4. (a-c) Power (solid) and accumulated dispersion (dashed) evolution in distance for the optimized numerical systems under test including OBP. (d-f) The corresponding NADD for each configuration.

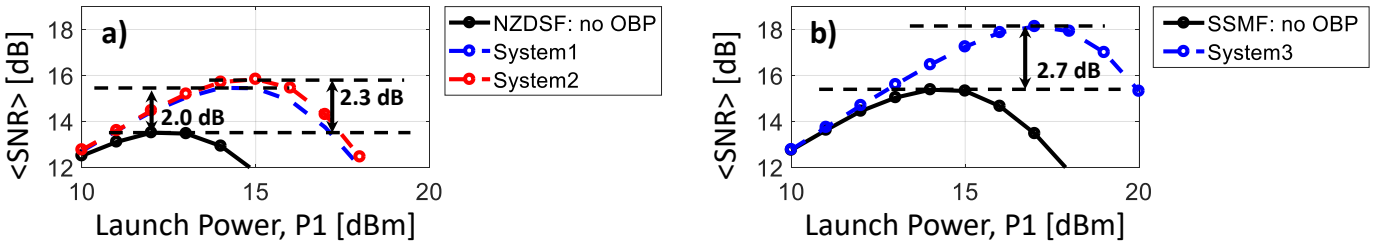

Fig. 5. Numerical SNR results for the central channel in seven-channel transmission as a function of the launch power into the link (P1) for the optimized systems with and without OBP: System1 and System2 (a), and System3 (b). Observe the presence of the dispersion-compensating module (not shown for visual clarity) between the two parts of the links.

To reduce the parameter space, the accumulated dispersion of the dispersion compensation unit (DA_2) is not explicitly optimized, but rather determined by the other parameters. It is also system-specific due to changes in the dispersion signs of the employed fibers. In particular, System1 (NZDSF+SSMF) uses positive dispersion fibers across the entire system, and we adjust the dispersion compensating unit such that the total accumulated dispersion before and after the OPC is identical:

$$DA_2^{(1)} = L_1D_1 - L_2D_2, \tag{24}$$

Here we assumed $L_2D_2 \leq L_1D_1$. On the other hand, System2 (NZDSF+DCF) and System3 (SSMF+DCF) use positive dispersion fiber in the link, followed by negative dispersion fiber for compensation. Consequently, the dispersion compensating unit is then adjusted to completely undo the link's dispersion:

$$DA_2^{(2,3)} = L_1D_1. \tag{25}$$

These design principles become more apparent when examining the pulse evolution and the respective NADDs,

This article has been accepted for publication in a future issue of this journal, but has not been fully edited. Content may change prior to final publication. Citation information: DOI 10.1109/JLT.2021.3121435, Journal of Lightwave Technology

as shown in Fig. 4. The maps are plotted at the optimum system parameters provided in Table II, where we also calculate and include the parameter β defined as:

$$\beta = \left| \frac{L_2 D_2}{L_1 D_1} \right|. \tag{26}$$

β is in the range of 0 to 1, and it ultimately defines the range of pulse shapes that are replicated inside the compensation fiber relative to the link. High β implies that the compensation fiber restores and reapplies the nonlinearity generated over the entire link, whereas low β means that only a small fraction of the nonlinearity is reproduced in the compensation fiber, though it can then be matched to the link much more accurately.

TABLE II
Optimum parameters for the three system types including OBP.

Type	P_1, dBm	P_2, dBm	L_1, km	L_2, km	β
System1	14.0	18.0	200	8.8	0.15
System2	15.0	20.4	200	1.5	0.15
System3	17.0	17.0	200	5.1	0.15

For all the optimized systems, the compensation modules constitute a small fraction of the link in terms of physical distance (L_2) or the restored range of pulse shapes ($\beta = 0.15$), and thus they only marginally contribute to the overall loss. All of the schemes assume exponential power decay both in the link and in the compensation fiber, whereas the accumulated dispersion evolution differs depending on the considered scheme. In System1, a fraction of the link's dispersion is compensated through the dispersion compensating unit, before being reversed by OPC, and restored back to zero in the positive-dispersion compensation fiber, achieving complete all-optical dispersion compensation, as shown in Fig. 4a. In System2 and System3, the accumulated dispersion of the link is instead completely compensated by the dispersion compensating unit, maintained at zero as the field is conjugated, and it subsequently accumulates with a negative sign in the compensation fiber, as shown in Fig. 4b-c. For such systems, the residual accumulated dispersion must be addressed digitally after detection.

These system designs allow for achieving approximate propagation symmetry between the link and the compensation fiber. As shown in the respective NADDs, roughly the same nonlinearity is induced over a similar range of pulse shapes across the relevant high-power regions, which allows for matching and cancellation of the induced nonlinearity. The degree of symmetry, however, varies depending on the considered system scenario. Due to exponential power decay in both spans, matching the slopes in NADD requires that the link and the compensation fiber have opposite dispersion signs [25], [32]–[34], which is the case for System2 and System3, though not for System1. Despite this limitation, and even though the OBP addresses only a small fraction of the link due to low β, substantial gains are still demonstrated for all three cases, as illustrated in Fig. 5.

The performance results are presented as a function of the launch power into the link (P_1), and the scenarios including compensation assume the optimized OBP, but with the launch power into the compensation fiber (P_2) increasing alongside P_1 to maintain an optimum power difference. The results for System1 and System2 are both provided in Fig. 5a, as they share identical link reference based on NZDSF. Whereas the results for System3 are given in Fig. 5b, and they are compared against an uncompensated SSMF-based link. The obtained gains due to OBP are substantial, and they reach up to 2.0 dB, 2.3 dB, and 2.7 dB in SNR for System1, System2 and System3, respectively, for seven-channel transmission. This SNR improvement is directly correlated to the symmetry in NADD, which is limited for System1, where the slopes are not matched correctly, and best in System3, where close-to-ideal matching has been achieved. Despite this variation, the designed compensation module yields significant gains for all three system types.

2) Experimental verification: To validate the effectiveness of the proposed OBP designs, System1 is implemented and tested experimentally using the setup in Fig. 3. Due to laboratory limitations, only two IQ modulators are now employed at the transmitter side to modulate seven WDM channels: one is used for the even and one for the odd channels, with independent data fed to the two modulators. This choice yields a higher transceiver noise, limiting the transmitter SNR to approx. 20 dB. The channels are centered around 1540 nm, placed on a 25-GHz grid and modulated with DP-16QAM data at 16 GBd, with DP transmission obtained through a polarization-multiplexing emulator. The link is now based on 210 km of NZDSF, similarly to System1, and the OBP module is implemented by means of:

- fiber Bragg grating (FBG) for lumped dispersion compensation ($DA_2^{(1)} \approx -560$ ps/nm) [40], [41];
- OPC based on FWM in HNLF;
- short SSMF spool for compensation ($L_2 = 10.25$ km).

The OPC is based on degenerate four-wave-mixing (FWM) in a strained highly nonlinear fiber (HNLF) using bidirectional loop configuration to ensure polarization insensitivity, as in [24], [26], [32], [42]–[44], and it is accompanied by a wavelength shift from 1540 nm to 1550 nm. The conversion efficiency in the HNLF is approx -6 dB, sufficient to yield a low back-to-back conversion penalty below 0.5 dB in SNR, which becomes negligible in transmission [45]–[47].

The system performance is maximized by optimizing the input powers into the link and into the compensation fiber, with the optimum achieved at $P_1 = 14.5$ dBm and $P_2 = 19.5$ dBm. The resulting power and dispersion evolution is plotted in Fig. 6a, alongside the achieved NADD in Fig. 6b. On top of the respective fiber parameters, these maps also incorporate the inherent wavelength shift from 1540 nm to 1550 nm due to the OPC, which affects the dispersion parameters of the waves in NZDSF and SSMF, as illustrated in Fig. 6c. Consequently, the signal traverses

This article has been accepted for publication in a future issue of this journal, but has not been fully edited. Content may change prior to final publication. Citation information: DOI 10.1109/JLT.2021.3121435, Journal of Lightwave Technology

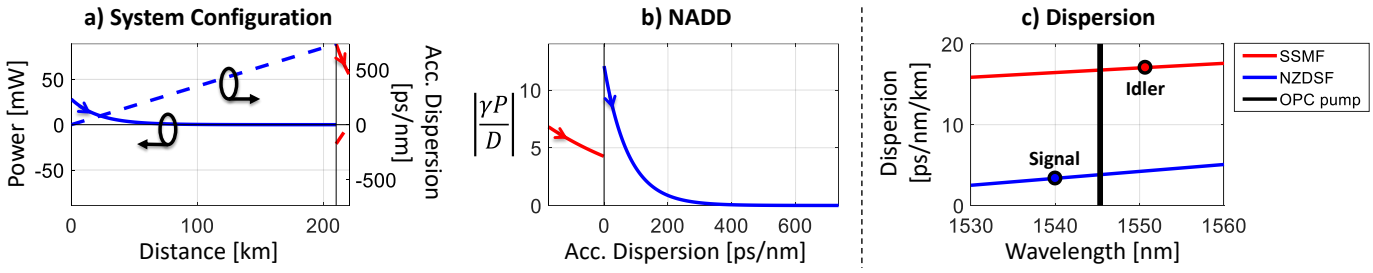

Fig. 6. a) Power and dispersion evolution in distance for the optimized experimental system with OBP, (b) resulting NADD, (c) dispersion characteristics of SSMF and NZDSF, with the signal, the OPC pump, and the idler wavelengths marked alongside.

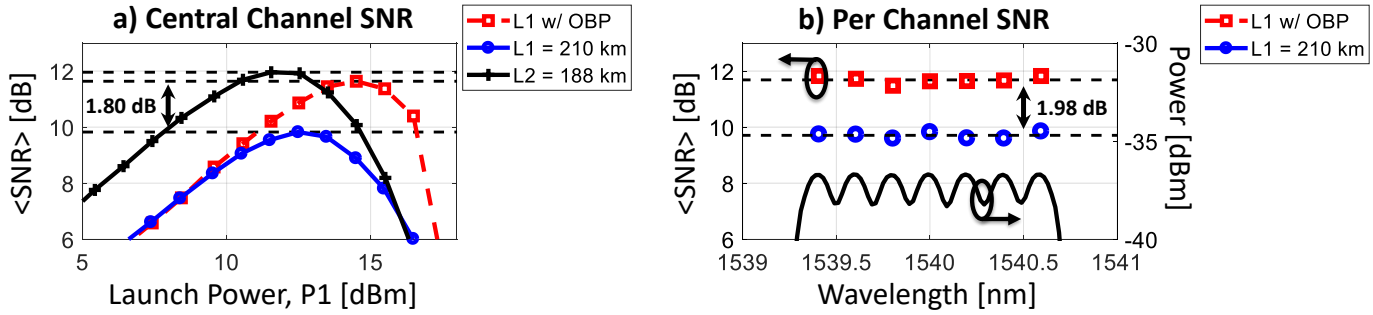

Fig. 7. (a) Experimental SNR of the central channel as a function of the launch power into the link, and (b) maximum SNR of all channels with and without OBP.

NZDSF experiencing $D_1(1540\text{ nm}) = 3.5$ ps/nm/km, and the conjugated idler then passes through SSMF with $D_2(1550\text{ nm}) = 17$ ps/nm/km. With these dispersion parameters and the chosen fiber lengths, the system achieves all-optical dispersion compensation in the end, and it has a $\beta \approx 0.24$, meaning that the OBP restores the pulse shapes and aims to reapply the nonlinearity of the initial 24% of the link. The value is dictated by the available equipment, and it is not far from the numerical optimum.

The experimental measurement results are presented in Fig. 7. They are obtained by varying the input power into the link (P_1), and then optimizing the power into the compensation fiber (P_2) at each point. As shown in Fig. 7a for the central channel, the OBP module leads to a shift of the optimum P_1 to higher powers, which is accompanied by an increase in the received SNR, indicating that the nonlinearity has been successfully compensated. For the optimized system, experimental gains of 1.8 dB in SNR are demonstrated for the central channel, and the 210-km link with OBP achieves almost the same performance as a shorter 188-km reference system, implying up to 12% reach enhancement thanks to compensation. Moreover, the measured SNR results are consistent across all seven WDM channels, as shown in Fig. 7b, with the average gain of 1.98 dB, which further outlines the applicability of this approach.

C. State of the art Raman-amplified systems

In this final section, we numerically apply the lumped compensation approach to a long-reach state-of-the art unrepeatered link with distributed and remote amplification. Contrary to OBP, here we focus on optical pre-compensation (OPreC) instead, meaning that we compensate the nonlinearity at the transmitter side before transmission. Placing of the compensation module was dictated by the link design, and it provides excellent propagation symmetry, while reducing the overall system complexity, as discussed next. Although in this section we provide a purely numerical study, it focuses on commercially available equipment, thus the analysis can be considered realistic and practical.

The complete transmission setup for the numerical analysis is sketched in Fig. 8 for the case without and with OPreC. Similarly to the previously discussed numerical systems, we use ideal LDs to generate seven WDM channels, which are subsequently modulated with IQ modulators, amplified, and combined. NFs of all EDFAs are again fixed at 5 dB. The channels are centered around 1550 nm on a 37.5 GHz grid, and each one carries DP-16QAM test data at 32 GBd per polarization. This signal is now optionally pre-distorted at the transmitter side using OPreC, which like OBP consists of three main components:

- DCF as a compensation fiber for pre-distortions;
- dispersion compensating unit for pulse shaping;
- OPC device for reversing the nonlinearity.

The DCF is forward-Raman pumped to finely tune the power profile and better control the symmetry of the system. The associated Raman noise is assumed uniform in frequency, and it is added at the output of the given fiber segment. The subsequent lumped dispersion compensating unit is designed to always compensate all of the

This article has been accepted for publication in a future issue of this journal, but has not been fully edited. Content may change prior to final publication. Citation information: DOI 10.1109/JLT.2021.3121435, Journal of Lightwave Technology

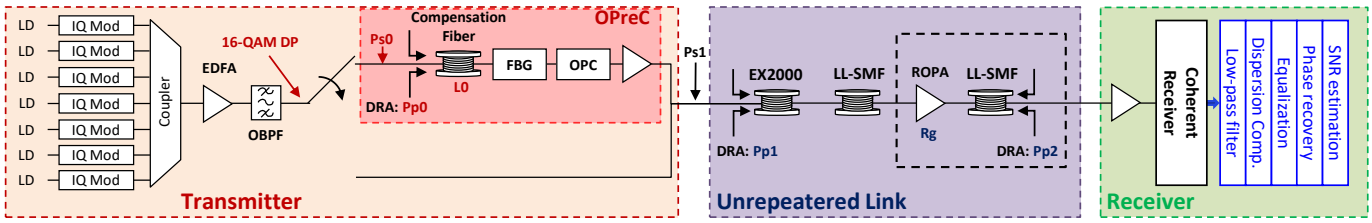

Fig. 8. Numerical setup for simulating long-reach Raman-amplified unrepeatered transmission including the proposed optical pre-compensation.

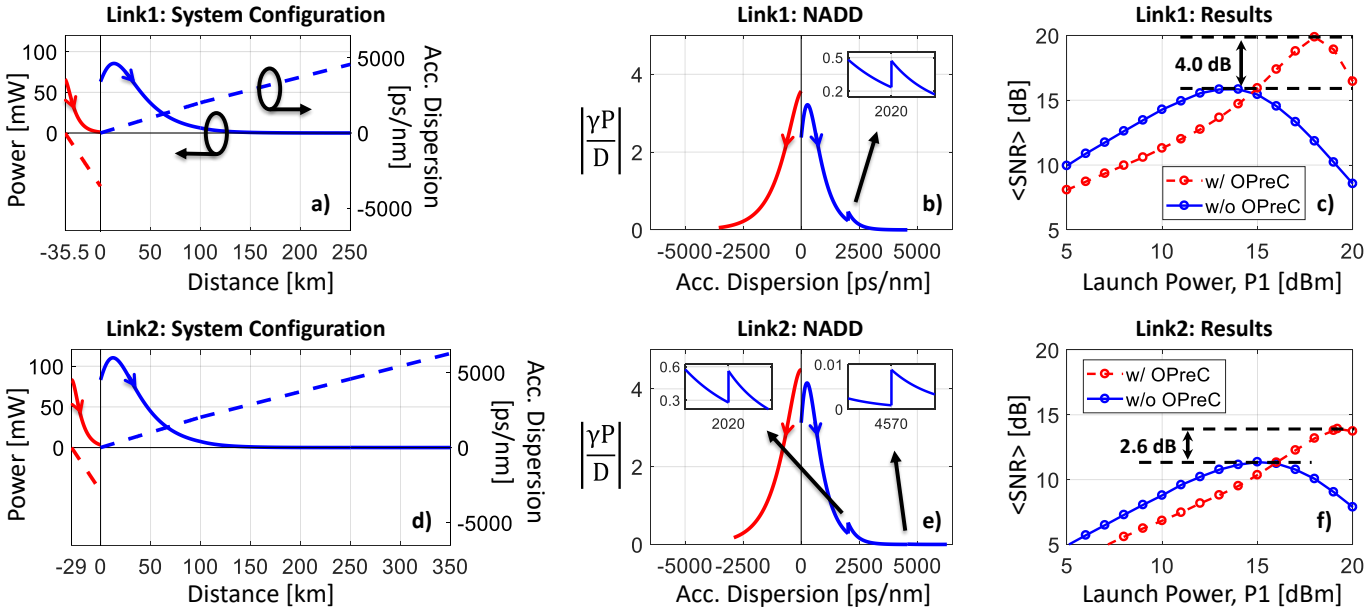

Fig. 9. (a,d) Power and dispersion evolution of the studied unrepeatered system including the proposed optical pre-compensation, (b,e) resulting NADD, (c,f) gains in SNR for numerical investigations of 250-km Link1 (a-c) and 350-km Link2 (d-f).

accumulated dispersion from the DCF, and it is followed by an OPC that is simulated using ideal conjugation of the field amplitude $A(z,t) \rightarrow A^*(z,t)$ with no wavelength shift or any additional penalty. This pre-distorted signal then enters one of the two analyzed unrepeatered transmission links: Link1 is made of 100 km of forward Raman-pumped large effective area fiber (EX2000) and 150 km of low-loss single-mode fiber (LL-SMF), whereas Link2 is the same as Link1, but it is extended thanks to an extra remote optically pumped amplifier (ROPA) and additional 100 km of backward Raman-pumped LL-SMF (dashed in Fig. 8). The relevant fiber parameters of both links are provided in Table III. Consequently, Link1 is 250-km, whereas Link2 is 350-km long in total, and they are both simulated using standard SSFM with an adaptive step size [28], [29], with the impact of PMD and higher order dispersion neglected. These links have been used for recent record transmission performance demonstrations [48]–[50], where the accuracy of the transmission model has also been verified. After traversing the link, the signal is detected using a standard receiver, and processed with a DSP chain. The processing includes digital dispersion compensation, as the link's dispersion is not addressed optically in this scheme, but it does not target nonlinearity compensation specifically.

TABLE III
Parameters of the fibers employed in the Raman-amplified system.

Type	α, dB/km	D, ps/nm/km	γ, 1/W/km	L, km
EX2000	0.16	20.2	0.76	100
LL-SMF	0.18	17.0	1.28	varied
DCF	0.50	-100.0	5.40	varied

The discussed links are optimized with regard to the received SNR of the central channel, and evaluated with and without compensation. It is assumed that every Raman-pumping stage in the systems consists of two equal-power pumps at 1452 nm and 1457 nm, and that each pump can deliver a maximum of 23 dBm power [48]–[50]. The pump powers for the DCF ($Pp0$) and EX2000 ($Pp1$) are included in the optimization process, whereas the backward pumping of the LL-SMF ($Pp2$) and the ROPA gain (R_g) are fixed to 23 dBm and 10 dB, respectively, as they do not significantly impact the symmetry of the system. Ultimately, for the case without OPreC, the parameter space reduces to only two variables:

- signal launch power into the link ($Ps1$),
- forward pumping power into the link ($Pp1$),

This article has been accepted for publication in a future issue of this journal, but has not been fully edited. Content may change prior to final publication. Citation information: DOI 10.1109/JLT.2021.3121435, Journal of Lightwave Technology

and these parameters can be easily optimized using a standard grid search. Whereas for the case including OPreC, proper symmetry design requires joint optimization of the following variables:

- signal launch power into the DCF ($Ps0$),
- forward pumping power into the DCF ($Pp0$),
- DCF length ($L0$),
- signal launch power into the link ($Ps1$),
- forward pumping power into the link ($Pp1$),

and it is conducted using the particle swarm optimization (PSO) algorithm to increase efficiency and speed of the process [51], [52]. The PSO optimization is conducted for 100 randomly initialized particles operating in parallel, with the acceleration coefficients $C1 = 1.2$, $C2 = 0.1$, and inertia $W = 0.05$. The parameters ensure that the step size is small enough, while providing reasonable convergence times. The optimization results for both links with and without OPreC are presented in Table IV.

TABLE IV
Optimized systems under test with and without OPreC.

	Link1 (250 km)		Link2 (350 km)	
Parameter	no OPreC	OPreC	no OPreC	OPreC
L_0, km	n/a	35.5	n/a	29.0
P_{s0}, dBm	n/a	18.2	n/a	19.2
P_{p0}, dBm	n/a	16.0	n/a	16.8
P_{s1}, dBm	14.0	18.0	15.0	19.2
P_{p1}, dBm	23.0	23.0	23.0	23.0
P_{p2}, dBm	n/a	n/a	23.0	23.0
R_g, dB	n/a	n/a	10.0	10.0

It is apparent from Table IV that the compensation modules tend to boost the optimum signal launch power into the link, as a consequence of the nonlinearity suppression. Moreover, the modules for both Link1 and Link2 are very similar, with the only major difference being an increase in P_{s0} and P_{s1} for the longer distance to counteract higher transmission losses and the increased ulamplified spontaneous emission (ASE) contribution, whereas the other parameters are only finely tuned to maximize the symmetry.

The optimized systems including OPreC are visualized in Fig. 9, alongside the resulting NADD and the performance gains. As shown in the system configurations, both links (right side) are characterized by only a single high-power region at the beginning of transmission, and this region is matched to in the pre-compensation module (left side). It is noted that the compensation fiber does not count towards transmission distance because lumped compensation is assumed in this scheme. Although the symmetry is not immediately clear from the system configurations, it is revealed immediately when examining the respective NADDs. On top of the symmetry, the NADDs also incorporate discontinuities at 100 km (2020 ps/nm) for both links due to change of fiber from EX2000 to LL-SMF, and at 250 km (4570 ps/nm) for Link2 due to lumped ROPA gain, as shown in the insets of Fig. 9b,e. This further outlines their efficiency in describing the nonlinearity accumulation.

Finally, the compensation gains for each of the systems are illustrated in Fig. 9c,f. The results are presented as a function of the signal launch power into the link ($Ps1$), with all the other parameters fixed to the optimum, as given in Table IV. For both Link1 and Link2, a penalty is observed as $Ps1$ deviates from the optimum. As the signal ($Ps0$) and Raman pump ($Pp0$) powers used for the compensation module are kept fixed at the optimal value for the optimum signal power into the link, for values of $Ps1$ lower (higher) than the optimum, the nonlinearity is overcompensated (undercompensated), yielding a mismatch and thus a performance penalty. With the powers tuned correctly, i.e. at optimum $Ps1$, however, the OPC symmetry is largely satisfied, as shown by NADDs, and substantial SNR improvement is demonstrated. At the optimum, the gains reach up to 4.0 dB for the shorter 250-km Link1, and up to 2.6 dB for the longer 350-km Link2. The lower improvement for Link2 is associated with a higher ASE contribution due to the additional link extension, as well as the uncompensated nonlinearity beyond the high-power region at the input to the link. These results give evidence that even links with complex power and dispersion profiles could be enhanced by lumped nonlinearity compensation, given that the module is properly designed.

IV. Conclusion

In this paper, we have presented and discussed principles of symmetry design allowing for analysis of lumped nonlinearity compensation, i.e. with the compensation performed in an additional transmitter- or receiver-based module that is not a part of the transmission link. We find this to be a promising approach to optical phase conjugation (OPC)-based compensation, which is particularly suitable for unrepeatered links where mid-span OPC cannot be performed. Ultimately, we demonstrated that using fibers with different combination of transmission properties allows for scaling down the physical extent of the compensation fiber while maintaining the symmetry required for OPC-based compensation. To enable this scaling, we here propose a new metric for symmetry evaluation, i.e. the nonlinearity versus accumulated dispersion diagram (NADD), which can be considered as a more general version of the power versus accumulated dispersion diagram (PADD), as it accounts for the induced nonlinear phase-shift rather than propagation power profile.

We have shown successful application of this method to several distinct unrepeatered systems with varying complexity:

1) Receiver-side compensation based on fiber types of the same dispersion sign for compensation and transmission in Section III-B;
2) Receiver-side compensation based on fiber types of opposite dispersion signs for compensation and transmission in Section III-B;

3) Transmitter-side compensation state-of-the-art Raman-amplified system in Section III-C.

For the former two links, we presented several possible designs of a receiver-side compensator, demonstrating up to 3.80 dB and 1.98 dB gains in SNR in a numerical and experimental investigation, respectively, for seven-channel transmission.We also tailored this compensation technique to a state-of-the-art long-reach Raman-amplified unrepeatered system considering transmitter-side compensation using a scaled-down compensation structure. . Despite the complicated power and dispersion profiles of the link, the numerical evaluation of our system revealed up to 4.0 dB gain in SNR for seven-channel WDM transmission.

It is evident that OPC-based compensation of nonlinearity can be applied in a lumped fashion by synthesizing propagation symmetry in scaled-down structures which are carefully matched to transmission links.Consequently, we find this to be a very powerful technique to designing optical compensation units for almost any link configuration. We furthermore believe that this approach might also enable potential upgrades to existing systems, where changing the link itself is undesirable or not possible at all.

Acknowledgment

DNRF Research CoE, SPOC (ref. DNRF123), the ERC CoG FRECOM (771878), the Villum YIP OPTIC-AI (29344), and OFS Denmark for providing the transmission fibers and the HNLFs.

References

[1] P.J. Winzer, D.T. Neilson and A.R. Chraplyvy, "Fiber-optic transmission and networking: the previous 20 and the next 20 years", Optics Express 26(18), 24190-24239 (2018).

[2] A.D. Ellis, M.E. McCarthy, M.A.Z. Al-Khateeb, M. Sorokina and N.J. Doran, "Performance limits in optical communications due to fiber nonlinearity", Adv. in Optics and Photonics 9(3), 429–503 (2017).

[3] F. Da Ros et al, "Characterization and Optical Compensation of LP01 and LP11 Intra-modal Nonlinearity in Few-Mode Fibers", Proc. OFC, paper Th1H.4 (2020).

[4] E. Ip and J.M. Kahn, "Compensation of dispersion and nonlinear impairments using digital backpropagation", J. Lightwave Technol. 26(20), 3416-3425 (2008).

[5] T. Umeki et al., "Simultaneous nonlinearity mitigation in 92 × 180Gbit/s PDM-16QAM transmission over 3840 km using PPLN-based guard-band-less optical phase conjugation", Optics Express, 24(15), 16946-16948 (2016).

[6] F. Da Ros et al., "Optical Phase Conjugation in a Silicon Waveguide with Lateral p-i-n Diode for Nonlinearity Compensation", J. Lightwave Technol. 37(2), 323-329 (2019).

[7] M. Morshed et al., "Experimental demonstrations of dual polarization CO-OFDM using mid-span spectral inversion for nonlinearity compensation", Optics Express 22(19), 10455–10466 (2014).

[8] H. Hu, R.M. Jopson, A.H. Gnauck, S. Randel and S. Chandrasekhar, "Fiber nonlinearity mitigation of WDM PDM QPSK/16-QAM signals using fiber-optic parametric amplifiers based multiple optical phase conjugations", Optics Express 25(3), 1618–1628 (2017).

[9] I. Sackey et al., "Kerr nonlinearity mitigation: mid-link spectral inversion versus digital backpropagation in 5 x 28-GBd PDM 16-QAM signal transmission", J. Lightwave Technol. 33(9), 1821–1827 (2015).

[10] I. Sackey et al., "Kerr nonlinearity mitigation in 5 × 28-GBd PDM 16-QAM signal transmission over a dispersion uncompensated link with backward-pumped distributed Raman amplification", Optics Express 22(22), 27381-27391 (2014).

[11] S. Watanabe, N. Takao, and C. Terumi, "Compensation of chromatic dispersion in a single-mode fiber by optical phase conjugation." IEEE Phot. Tech. Lett. 5(1), 92-95 (1993).

[12] Shu Namiki, Hung Nguyen Tan, Karen Solis-Trapala, Takashi Inoue "Signal-transparent wavelength conversion and light-speed back propagation through fiber", Proc. OFC, paper Th4F.1 (2016)

[13] A. A. I. Ali, T. T. Nguyen, S. Boscolo, S. Takasaka, R. Sugizaki, A. D. Ellis "Reduced Impact of Frequency Dithering on the Performance of High-Order Modulation Format Phase Conjugation" Proc. OFC, paper F1B.4 (2021)

[14] T. Umeki, T. Kobayashi, A. Sano, T. Ikut, M. Abe, T. Kazama, K. Enbutsu, R. Kasahara, Y. Miyamoto "Nonlinearity Mitigation of PDM-16QAM Signals Using Multiple CSI-OPCs in Ultra-Long-Haul Transmission without Excess Penalty" IEICE TRANSACTIONS on Communications, E103-B(11), 1226-1232 (2020)

[15] M.A.Z. Al-Khateeb, M.E. McCarthy, C. Sanchez and A.D. Ellis, "Nonlinearity compensation using optical phase conjugation deployed in discretely amplified transmission systems", Optics Express 26(18), 23945-23959 (2018).

[16] S. Yoshima et al., "Mitigation of nonlinear effects on WDM QAM signals enabled by optical phase conjugation with efficient bandwidth utilization", J. Lightwave Technol. 35(4), 971 - 978 (2017).

[17] C. Sanchez, E. McCarthy, A.D. Ellis, P. Wright and A. Lord, "Optical-phase conjugation nonlinearity compensation in Flexi-Grid optical networks", Proc. Recent Advances on Systems, Signals, Control, Communications and Computers, 39-43 (2015).

[18] X. Liang, S. Kumar and J. Shao, "Ideal optical backpropagation of scalar NLSE using dispersion-decreasing fibers for WDM transmission", Optics Express 21(23), 28668-28675 (2013).

[19] X. Liang and S. Kumar, "Optical back propagation for fiber optic networks with hybrid EDFA Raman amplification", Optics Express 25(5), 5031-5043 (2017).

[20] J. Shao, and S. Kumar. "Optical backpropagation for fiber-optic communications using optical phase conjugation at the receiver." Optics letters 37(15), 3012-3014 (2012).

[21] E. Bidaki and S.Kumar, "A Raman-Pumped Dispersion and Nonlinearity Compensating Fiber For Fiber Optic Communications", IEEE Photonics Journal 12(1), 1-17 (2019).

[22] M.D. Pelusi, "Fiber looped phase conjugation of polarization multiplexed signals for pre-compensation of fiber nonlinearity effect", Optics Express 21(18), 21423-21432 (2013).

[23] M.D. Pelusi and B.J. Eggleton, "Optically tunable compensation of nonlinear signal distortion in optical fiber by end-span optical phase conjugation", Optics Express 20(7), 8015-8023 (2012).

[24] P.M. Kaminski et al., "Nonlinear Phase-Shift Cancellation in Dispersion-Shifted Fiber Transmission by All-Optical Back-Propagation", Proc. CLEO, paper STu3L.2 (2020).

[25] P.M. Kaminski et al., "All-Optical Nonlinear Pre-Compensation of Long-Reach Unrepeatered Systems", Proc. ECOC, paper Tu1F.1 (2020).

[26] P.M. Kaminski et al., "Unrepeatered transmission reach extension by receiver-side all-optical back-propagation", Proc. OECC, paper MB1.4 (2019).

[27] G.P. Agrawal, "Fiber-Optic Communication Systems", 4^{th} Edition, Wiley (2010).

[28] G.P. Agrawal, "Nonlinear Fiber Optics", 5^{th} Edition, Elsevier Academic Press, Oxford (2013).

[29] O.V. Sinkin, R. Holzlöhner, J. Zweck and C.R. Menyuk, "Optimization of the Split-Step Fourier Method in Modeling Optical-Fiber Communications Systems", J. Lightwave Technol. 21(1), 61 - 68 (2003).

[30] G.H. Weiss and A.A. Maradudin, "The Baker-Hausdorff Formula and a Problem in Crystal Physics", J. Mathematical Physics 3(771), 61 - 68 (1962).

[31] S. Watanabe and M. Shirasaki, "Exact Compensation for both Chromatic Dispersion and Kerr Effect in a Transmission Fiber Using Optical Phase Conjugation", J. Lightwave Technol. 14(3), 243 - 248 (1996).

[32] P.M. Kaminski et al., "Symmetry Enhancement Through Advanced Dispersion Mapping in OPC-Aided Transmission", J. Lightwave Technol. PP, 1 - 1 (2021).

[33] P.M. Kaminski et al., "Enhanced dispersion mapping for OPC-aided transmission systems", Proc. ECOC, paper P101 (2019).

[34] P.M. Kaminski et al., "Improved nonlinearity compensation of OPC-aided EDFA-amplified transmission by enhanced dispersion mapping", Proc. CLEO, paper STu3L.4 (2020).

[35] P. Minzioni, F. Alberti, and A. Schiffini, "Techniques for Nonlinearity Cancellation Into Embedded Links by Optical Phase Conjugation", J. Lightwave Technol. 23(8), 2364 - 2370 (2005).

[36] M.E. McCarthy, M.A.Z.Al Kahteeb, F.M. Ferreira and A.D. Ellis, "PMD tolerant nonlinear compensation using in-line phase conjugation", Optics Express 24(4), 3385-3392 (2016).

[37] P. Minzioni, "Nonlinearity Compensation in a Fiber-Optic Link by Optical Phase Conjugation", Fiber Int. Optics 28(3), 179-209 (2009).

[38] P. Minzioni and A. Schiffini, "Unifying theory of compensation techniques for intrachannel nonlinear effects", Optics Express 13(21), 8460-8468 (2005).

[39] M.P. Yankov et al., "Constellation shaping for WDM systems using 256QAM/1024QAM with probabilistic optimization", J. Lightwave Technol. 34(22), 5146-5156 (2016).

[40] I. Kim, O. Vassilieva, Y. Akasaka, P. Palacharla and T. Ikeuchi, "Enhanced Spectral Inversion for Fiber Nonlinearity Mitigation", IEEE Photonics Technol. Letters 30(23), 2040-2043 (2018).

[41] O. Ozolins et al., "112 Gbps/λ PAM4 Inter-DCI with Continuous-Fiber Bragg Grating based Dispersion Compensators", Proc. Adv. Photonics, paper NeTh3F.3 (2018).

[42] I. Sackey et al., "Design and Performance Evaluation of an OPC Device Using a Dual-Pump Polarization-Independent FOPA", Proc. ECOC, paper Tu.1.4.4 (2014).

[43] T. Richter, R. Elschner, A. Gandhe, K. Petermann and C. Schubert, "Parametric Amplification and Wavelength Conversion of Single- and Dual-Polarization DQPSK Signals", IEEE Journal of Selected Topics in Quantum Electronics 18(2), 988 - 995 (2012).

[44] M.F.C. Stephens, M. Tan, I.D. Phillips, S. Sygletos, P. Harper and N.J. Doran, "1 THz-Bandwidth Polarization-Diverse Optical Phase Conjugation of 10x114Gb/s DP-QPSK WDM Signals", Proc. OFC, paper W3F.6 (2014).

[45] P.M. Kaminski et al., "Signal-to-Idler Conversion Penalty in AlGaAs-on-Insulator Wavelength Converter", Proc. CLEO, paper Stu4C.6 (2018).

[46] P.M. Kaminski et al., "Characterization and Optimization of Four-Wave-Mixing Wavelength Conversion System", J. Lightwave Technol. 37(21), 5628 - 5636 (2019).

[47] M.P. Yankov, P.M. Kaminski, F. Da Ros, "Four-wave mixing conversion efficiency requirements for optical phase conjugation based fiber nonlinearity compensation", Proc. CLEO, paper STu3L.1 (2020).

[48] J.H.C. Júnior, T.Sutili, S.M. Rossi, R.C. Figueiredo and D.A.A. Mello, "Fast Adaptive Digital Back-Propagation Algorithm for Unrepeatered Optical Systems", Proc. OFC, paper T4I.2 (2020).

[49] J.C.S.S. Januario, M.S. Rossi and H.C. Hose, "Unrepeatered WDM Transmission of Single-Carrier 400G (66-GBd PDM-6QAM) over 403 km", Proc. OFC, paper Th4D.1 (2017).

[50] T. Sutili, P.F.P. Neto, F.D. Simões, G.J. Suzigan and R.C. Figueiredo, "Cost-Effective Solution for High-Capacity Unrepeatered Transmission", Proc. OFC, paper T4I.4 (2020).

[51] R.C. Eberhart and Y. Shi, "Particle Swarm Optimization: Developments, Applications and Resources", Proc. IEEE Congr. Evolutionary Computation, 23-30 (2001).

[52] F.L.D. Lucia, J.H.C. Júnior, T. Sutili and R.C. Figueiredo, "Natural Computing Algorithms for Optimization of High-Order Distributed Raman Amplifiers", Proc. IMOC (2019).